# General purpose deep learning attenuation correction improves diagnostic accuracy of SPECT MPI: multicenter study

Running title: Generalizable virtual attenuation correction for SPECT

Aakash D. Shanbhag MSc[1,2], Robert J.H. Miller MD[3], Mark Lemley BS[1], Paul Kavanagh MSc[1], Joanna X. Liang MPH[1], Anna M Marcinkiewicz MD, PhD[1,4], Valerie Builoff BSc[1], Serge Van Kriekinge PhD[1], Terrence D. Ruddy MD[5], Mathews B. Fish MD[6], Andrew J. Einstein MD, PhD[7], Monica Martins MSc[8], Julian P Halcox MD[8], Philipp A. Kaufmann MD[9], Christopher Buckley PhD[10], Timothy M. Bateman MD[11], Daniel S. Berman MD[1], Damini Dey PhD[1], Piotr J. Slomka PhD[1]

1. Departments of Medicine (Division of Artificial Intelligence in Medicine), Imaging and Biomedical Sciences, Cedars-Sinai Medical Center, Los Angeles, CA, USA
2. Signal and Image Processing Institute, Ming Hsieh Department of Electrical and Computer Engineering, University of Southern California, Los Angeles, CA, USA
3. Department of Cardiac Sciences, University of Calgary, Calgary AB, Canada
4. Center of Radiological Diagnostics, National Medical Institute of the Ministry of the Interior and Administration, Warsaw, Poland
5. Division of Cardiology, University of Ottawa Heart Institute, Ottawa, Ontario, Canada
6. Oregon Heart and Vascular Institute, Sacred Heart Medical Center, Springfield, OR, USA
7. Division of Cardiology, Department of Medicine, and Department of Radiology, Columbia University Irving Medical Center and New York-Presbyterian Hospital, New York, NY, USA
8. Swansea University Medical School, Swansea University, Swansea, UK
9. Department of Nuclear Medicine, Cardiac Imaging, University Hospital Zurich, Zurich, Switzerland
10. GE Healthcare, Pollards Wood, Buckinghamshire, HP8 4SP, UK
11. Cardiovascular Imaging Technologies LLC, Kansas City, MO, USA, and the Saint Luke's Health System, Kansas City, MO, USA.

**Word count**: 4858 (including all elements)

**Funding:** This research was supported in part by grants R01HL089765 and R35HL161195 from the National Heart, Lung, and Blood Institute/ National Institutes of Health (NHLBI/NIH) (PI: Piotr Slomka). The content is solely the responsibility of the authors and does not necessarily represent the official views of the National Institutes of Health.

**Disclosure:** Dr. Robert Miller has received consulting fees and research support from Pfizer. Drs. Berman and Slomka and Mr. Kavanagh participate in software royalties for QPS software at Cedars-Sinai Medical Center. Dr. Marcinkiewicz received consulting fees from APQ health. Dr. Berman is a consultant for GE Healthcare. Dr. Einstein has received a speaker's fee from Ionetix, consulting fees from W. L. Gore & Associates and Artrya, authorship fees from Wolters Kluwer Healthcare—UpToDate, and served on a scientific advisory board for Canon Medical Systems USA; his institution has grants/grants pending from Attralus, BridgeBio, Canon

Medical Systems USA, GE HealthCare, Intellia Therapeutics, Ionis Pharmaceuticals, Mediwhale, Neovasc, Pfizer, Roche Medical Systems, and W. L. Gore & Associates. Dr. Slomka has received research grant support from Siemens Medical Systems and has received consulting fees from Synektik, SA. Dr. Ruddy received research grant support from GE Healthcare, Siemens Healthcare Limited, Pfizer Global and Canadian Medical Isotope Ecosystem. Dr. Buckley is an employee of GE Healthcare. Dr. Bateman has received consulting fees from GEHC and Synektik and receives royalties for the Imagen line of SPECT and PET software products. The remaining authors have no relevant disclosures.

**Address for correspondence:**

Piotr J. Slomka, PhD

Cedars-Sinai Medical Center

6500 Wilshire Blvd

Los Angeles, CA 90048

Email: Piotr.Slomka@cshs.org

**ABSTRACT (250/250 words)**

**Background**
Single photon emission computed tomography(SPECT) myocardial perfusion imaging(MPI) uses computed tomography(CT)–based attenuation correction(AC) to improve diagnostic accuracy. Deep-learning (DL) has the potential to generate synthetic AC images, as an alternative to CT-based AC.

**Objectives**
This study evaluates whether DL-generated synthetic SPECT images could enhance accuracy of conventional SPECT MPI.

**Methods**
We developed a DL model in a multicenter cohort of 4894 patients from 4 sites to generate simulated SPECT AC images(DeepAC). The model was externally validated in 746 patients from 72 sites in a clinical trial (NCT01347710) and 320 patients from another external site. In the first external population, we assessed the diagnostic accuracy for obstructive coronary artery disease (CAD)—defined as left main stenosis ≥50% or ≥70% in other vessels—for total perfusion deficit (TPD). In the latter, we completed change analysis and compared quantitative scores for AC, DeepAC, and non-attenuation correction (NC) with clinical scores.

**Results**
In the first external cohort (mean age 63 ± 9.5, 69.0% male), 206 patients(27.6%) had obstructive CAD. The area under the receiver operating characteristic curve (AUC) of DeepAC TPD (0.77, 95% confidence interval [CI] 0.73 – 0.81) was higher than NC TPD (AUC 0.73, 95% CI 0.69 – 0.77, $p<0.001$). In the second external cohort, DeepAC quantitative scores had closer agreement with actual AC scores compared to NC.

**Conclusion**
In a multicenter external population, DeepAC improved prediction performance for obstructive CAD. This approach could enhance diagnostic accuracy in facilities using conventional SPECT systems, without requiring additional equipment, imaging time or radiation exposure.

**KEYWORDS:**
attenuation correction, SPECT, myocardial perfusion imaging, deep learning, artificial intelligence

**ABBREVIATIONS:**

CAD – coronary artery disease

SPECT- single photon emission computed tomography

MPI – myocardial perfusion imaging

NC- non attenuation correction

AC- attenuation correction

SSS – summed stress score

TPD- total perfusion deficit

AUC - area under the receiver operating characteristic curve

DL- deep learning

cGAN – conditional generative adversarial network

## INTRODUCTION

Myocardial perfusion imaging (MPI) is one of the most commonly ordered diagnostic tests for evaluation of coronary artery disease (CAD)[1]. There is a wealth of knowledge demonstrating that computed tomography (CT)-based attenuation correction (AC) can improve diagnostic accuracy by improving specificity[2-4]. However, the majority of MPI is performed in community labs without hybrid single photon emission computed tomography (SPECT)/CT camera systems and therefore without AC imaging[4]. The need for methods to provide AC for non-hybrid systems is widely recognized by the cardiac imaging community[3].

Deep learning (DL) offers the potential to generate synthetic AC images though a variety of approaches[5-8]. Direct approaches use DL models to generate either synthetic AC polar map images or synthetic SPECT images[6,7], while indirect approaches involve an intermediate step of creating a synthetic AC map[5], which is then used to infer AC images. We previously developed a DL model that directly generated synthetic AC SPECT images (without intermediate synthetic AC map generation), demonstrating superior diagnostic accuracy compared to non-AC imaging and similar accuracy to actual AC imaging[8]. The advantage of the direct approach is does not require additional reconstruction and can be performed rapidly as a post processing step. However, our previous study only evaluated performance on one type of solid-state SPECT camera system. DeepAC SPECT image generation could potentially be applied to images from conventional SPECT camera systems or other solid-state camera systems. Failure to demonstrate broad clinical utility of these approaches is one reason for clinical skepticism regarding this potentially groundbreaking and practical application of artificial intelligence. Importantly, synthetic AC images could be used to improve diagnostic accuracy for the 74% of studies

performed worldwide without CT-based AC[9], with no added imaging time or radiation exposure.

In this work, we trained a general purpose DeepAC model using a variety of SPECT/CT systems and tested the model in both a cohort of patients imaged with conventional SPECT camera systems from a prospective multicenter study and an external population with available CT based AC images.

## MATERIALS AND METHODS

### Patient Populations

This study includes one training population and two external testing populations. The training population was derived from a multicenter registry of patients undergoing SPECT/CT MPI[10,11]. The protocol was approved by research ethics boards at each site, including either written informed consent or waiver of informed consent for use of retrospective data. The overall registry was reviewed and approved by the institutional review board at Cedars-Sinai Medical Center. The first external population was derived from a phase III multi-center clinical trial (NCT01347710) and included patients with known or suspected CAD who were referred for clinically indicated invasive coronary angiography (ICA) between June 2011 and September 2013 across 72 clinical sites in 3 countries (the USA, Canada, and Finland)[12]. This population was used to evaluate the model's performance in predicting obstructive CAD. Approval was obtained from research ethics boards at each trial site, written informed consent was obtained prior to participation in the trial, and the study complied with the Declaration of Helsinki. The second external population included patients from Cardiovascular Imaging Technologies LLC and the Saint Lukes Health System (Kansas City, MO) with stress and rest non AC and AC

scans. This population was used to compare quantitative summed scores derived using DeepAC to actual AC and non-AC values. Study methodology is summarized in the **Central Illustration**.

Image Acquisition

Image acquisition is outlined in the supplemental methods[12-15].

Visual analysis

Visual interpretation of cases is outlined in the supplemental methods[12] [16].

Model Architecture

We trained a new generalizable DeepAC model using the architecture which has been previously described(8). In brief, the model utilized a conditional generative adversarial network (cGAN), with the generator model being a modified U-Net. The model was trained using 4894 (training: 4402, validation: 492) pairs of non attenuation correction (NC) and AC short axis SPECT slices from stress acquisitions. For homogeneity in training with different cameras, resampling to common 4 x 4 x 4mm template with mean normalization was carried out. The model generated DeepAC SPECT image volumes which were then processed using conventional interpretation software to derive DeepAC polar maps.

Quantitative Image Analysis

All quantitative image comparisons were performed in the external testing population. Stress total perfusion deficit (TPD) was quantified with Quantitative Perfusion SPECT (QPS) software (Cedars-Sinai Medical Center, Los Angeles, CA)[17]. Sex and camera-specific normal limits were used for quantification of NC images. Quantification of TPD and quantitative summed stress scores (SSS) for DeepAC images was performed using normal limits created

from DeepAC corrections of the same normal cases used to derive sex-specific and camera-specific databases for NC studies. Quantitative SSS and summed rest scores (SRS) were calculated from polar maps[17]. Additionally, change analysis was used to perform voxel-by-voxel comparisons between AC images, NC images, and DeepAC images in External Testing Population 2[18]. Positive change reflects an increase in counts in regions of the reference polar map[18].

Diagnostic Accuracy for Obstructive CAD

Obstructive CAD was defined as stenosis ≥70% in any coronary artery, or ≥50% in the left main coronary artery. Diagnostic accuracy was evaluated on a per-vessel basis, with left main disease attributed to both the left anterior descending (LAD) and left circumflex (LCx) territories. Improvement in specificity at 80% sensitivity for DeepAC was compared to NC.

Statistical Analysis

Standard descriptive statistics were used. Normality for continuous variables was assessed with the Shapiro-Wilks test. Continuous variables were not found to have a normal distribution and difference in median was assessed using the Wilcoxon signed-rank test. Diagnostic accuracy of obstructive CAD was assessed using the area under the receiver operating characteristic curve (AUC). DeLong's test was used to evaluate differences in AUC[19]. We compared clinical SSS with quantitative SSS using Bland-Altman analysis including mean difference and limits of agreement. Differences in limits of agreement were assessed using an F-test. All statistical tests were two-sided with p-value<0.05 considered significant. Statistical analyses were performed using R (version 4.1.2) and Stata version 13.0 (StataCorp, College Station, Texas, USA).

## RESULTS

### Training and Validation population

A summary of the training and validation population as well as two external testing populations is included in **Table 1.** In total, 4894 patients were included in the training and validation populations as shown in **Supplemental Table 1**. The median age was 65 with interquartile range (IQR) 57-73, 52% were male, 54% had hypertension, 21% had a history of diabetes mellitus, and 35% had dyslipidemia.

### External Testing Population 1 – Phase III Clinical Trial

In total 746 patients from a phase III clinical trial were included in the first external testing population with median age 63 (IQR 56-69) and 515 (69%) male. Obstructive CAD was present in 206 (27.6%) of patients, with patient characteristics shown in **Supplemental Table 2**. Patients with obstructive CAD were older (median age 65 vs 62, $p<0.001$), more likely to be male (85% vs 63%, $p<0.001$), and were more likely to have a history of diabetes (45% vs 30%, $p<0.001$) or dyslipidemia (92% vs 84%, $p=0.008$). Patients with obstructive CAD had significantly higher DeepAC TPD (median 7.81 IQR [3.61, 14.0] vs 2.25 [0.77, 4.40], $p<0.001$) and NC (median 9.56 IQR [4.07, 15.8] vs 3.23 [0.99, 7.32], $p<0.001$).

### Prediction Performance for Obstructive CAD in external testing population 1

Prediction performance for obstructive CAD is shown in **Figure 1.** The AUC of DeepAC TPD (0.768, 95% confidence interval [CI] 0.730 – 0.807) was significantly higher than NC TPD (AUC 0.727, 95% CI 0.686 – 0.768, $p<0.001$) and two of three reader interpretations. At 80% sensitivity, there was improved specificity for DeepAC TPD (60.7%, 95 % CI 0.55-0.65)

compared to NC TPD (50.2%, 95% CI 0.47-0.56, p<0.001). For SSS ≥ 4, specificity for DeepAC (74.6%, 95% CI 0.71-0.78) was significantly higher compared to NC (60.2%, 95% CI 0.56-0.64, p<0.001) and comparable to all three readers (Reader 1 p=0.696 , Reader 2 p=0.461, Reader 3 p=0.711), while sensitivity of DeepAC (66.7%, 95% CI 0.60-0.73) was comparable to NC (70.7%, 95% CI 0.64-0.76, p=0.175).

DeepAC TPD had the highest prediction performance for obstructive CAD in both female patients (AUC 0.745) and male patients (AUC 0.760) (**Supplemental Figure 1**). The improvements in prediction performance were also seen in patients with elevated body mass index (BMI) (≥30 kg/$m^2$) or non-elevated BMI (**Figure 2**). In patients undergoing exercise stress, DeepAC had the highest prediction performance (AUC 0.851, 95% CI 0.791 – 0.911, p<0.05 compared to NC TPD and all readers) (**Figure 3**). While in patients undergoing pharmacologic stress, DeepAC TPD had the highest prediction performance numerically (AUC 0.733, 95% CI 0.686 – 0.871), but only significantly outperformed reader 2 (AUC 0.682, 95% CI 0.637 – 0.726, p=0.022).

Obstructive CAD was present in the LAD distribution in 81 (11%) patients, the LCx distribution in 82 (11%) patients and the right coronary artery in 97 (13%) patients. Per-vessel prediction performance for NC stress TPD and DeepAC TPD is shown in **Supplemental Figure 2.** There was no significant difference in per-vessel prediction performance. We further stratified the per-vessel analysis by mode of stress (**Supplemental Table 3**). In this analysis, per-vessel prediction performance improved in the RCA territory in patients undergoing exercise stress (DeepAC AUC 0.902 vs NC AUC 0.837, p=0.031), but not in other vessels or in patients undergoing pharmacologic stress.

Case Example:

**Figure 4** shows images from a 61-year-old female patient with a BMI of 30 kg/m$^2$. One reader interpreted the scan as definitely abnormal and the remaining two readers as definitely normal. NC TPD was elevated at 8%. DeepAC images show only mild abnormality, with 3% TPD. Invasive coronary angiography demonstrated no-obstructive CAD. The defect was most likely a diaphragmatic attenuation artifact.

Comparison to CT-based AC

The External Testing Population 2 included 320 patients, median age 61 (IQR 54, 68), and 126 (39%) male. Change analyses for stress and rest are shown in **Figure 5.** The positive change between stress AC and DeepAC (median 3.49%, IQR 2.06 – 5.09) was substantially lower compared the positive change between stress AC and NC (median 10.3%, IQR 5.7 – 14.2, $p<0.001$). This reflects less of a polar map defect for DeepAC compared to the defect seen on NC when AC polar maps are used as the reference standard. Similar results were seen for positive change of rest polar maps.

The mean difference between AC and DeepAC SSS was -1.13, with limits of agreement -5.62 to 3.35. In comparison, the mean difference between AC and NC was -1.14 but with limits of agreement -7.02 to 4.73. Variance was lower between AC and DeepAC compared to AC vs NC ($p<0.001$). The mean difference between AC and DeepAC SRS was -0.25, with limits of agreement -3.28 to 2.78. The mean difference between AC and NC SRS was -0.53, with limits of agreement -4.30 to 3.23. Variance was lower between AC and DeepAC compared to AC vs NC ($p<0.001$). Comparison between clinical SSS and SRS vs quantitative SSS and SRS for AC and DeepAC are shown in **Supplemental Figure 3.**

Case Example

A 57-year-old female patient with high body mass index of 38 kg/m$^2$ with available CT based AC shown in **Figure 6**. NC total perfusion deficit (TPD) was abnormal at 8% and summed stress score was 4. Both CT AC images and DeepAC images demonstrated no perfusion abnormalities (stress TPD 0%, summed stress score 0).

**Figure 7** shows images from a 68-year-old female patient with high body mass index of 52 kg/m$^2$ from External Testing Population 2. All methods for quantitation were abnormal, with summed stress scores of 9 for CT AC, 14 for DeepAC, and 16 for NC imaging. Reader interpretation was definitely abnormal with SSS of 25.

## DISCUSSION

We evaluated the performance of our generalized conditional GAN-based DeepAC model developed on multicenter data using two large external populations. We found that the prediction performance for DeepAC TPD, externally tested in a cohort of patients imaged with conventional SPECT camera systems from a prospective multicenter study, was significantly improved compared to NC TPD. DeepAC also outperformed expert readers, with at least numerically superior accuracy overall and across all subgroups of interest, and statistically significant performance improvement on 2 out 3 readers. We also demonstrated that DeepAC images were more similar to actual AC images compared to NC images in a second external cohort imaged with SPECT/CT camera systems. The generation of DeepAC SPECT images allows physicians to directly compare SPECT images, ensuring that DeepAC corrects attenuation artifacts without over-correcting true defects. These results suggest that DeepAC could be

implemented in labs without access to SPECT/CT camera systems to significantly improve the diagnostic accuracy of MPI.

The need for artificial intelligence solutions for synthetic AC image generation has been broadly acknowledged with several groups suggesting different solutions. Chen et al. developed a DL network incorporating gender, BMI, scatter window images, and non AC images to predict AC images[20], with images more similar to actual AC compared to a standard U-Net model. Nguyen et al. utilized a GAN to simulate AC images from non AC data, achieving a structural similarity index of 0.946 compared to true AC images, outperforming U-Net alone[21]. It may also be possible to provide synthetic AC correction in the presence of significant gross patient motion[22]. Synthetic AC image also has potential advantages over CT-based AC including the absence of potential artifacts from misregistration.

While the technical performance of synthetic AC imaging is important to evaluate, diagnostic accuracy remains the most crucial clinical evaluation. Hagio et al. investigated synthetic AC polar maps from non AC polar maps using convolutional neural networks[23]. This approach was applied to 722 patients (from the same set of trial data as the current study), with improvements in AUC from 0.717 to 0.752 for quantitative perfusion[7]. In the present study, using a slightly larger population, we were able to demonstrate improvements in AUC from 0.731 to 0.768 with the use of DeepAC TPD from entire volumes instead of polar maps, as well validate on an additional external site with CT AC. DeepAC corrects SPECT image sets directly; therefore, cases with segmentation errors that could hamper polar map AC generation did not need to be excluded. Additionally, we have previously established that AC with deep learning-based synthetic SPECT imaging outperforms synthetic polar maps[24]. Direct image to image AC generation leverages optimized vendor-specific reconstruction algorithms for dedicated

collimators and solid-state scanners. Lastly, this approach allows physicians to evaluate full image sets for potential artifacts using the same approach they would for any other clinical study. Importantly, the improvements in accuracy demonstrated in the present study are similar to those achieved from actual AC imaging(25), without the need for a CT image acquisition with associated radiation exposure.

The multicenter nature of this analysis allowed us to evaluate the external performance of our model, including accuracy across important subgroups. We found that DeepAC had the highest prediction performance regardless of sex, body habitus, or stress protocol. The improvement in prediction performance for DeepAC compared to NC was significant in patients undergoing exercise stress but not in patients undergoing pharmacologic stress. This may be related to more pronounced diaphragmatic artifacts in patients undergoing exercise stress or prominent subdiaphragmatic radiotracer activity in patients undergoing pharmacologic stress leading to overcorrection (and minimizing the benefits of DeepAC)(26). Regardless, we did not identify any subgroups or vascular territories in which DeepAC had lower prediction performance compared to NC or any of the expert readers. Further investigation with a larger sample size of patients undergoing pharmacologic stress or pharmacologic stress with low-level exercise would be beneficial to fully understand this effect. However, we also saw significant variability in prediction performance of readers across sub-groups. For example, Reader 3 had the highest accuracy among the expert interpreters, but had lower prediction performance in female patients and in patients with a normal body habitus. Conversely, Reader 2 had the lowest accuracy amongst the expert readers but the highest prediction performance in female patients. These variabilities between readers suggest that methods to support diagnostic interpretation,

including DeepAC image sets and quantitative analysis, are needed to help overcome potentially biased interpretation patterns.

In the present work, we also completed additional technical evaluations of our approach. In our previous work, which only included patients imaged with Discovery 530 or 570 camera systems, we demonstrated lower positive change between AC and DeepAC compared to the change between AC and NC. In the current analysis, we also demonstrated lower positive change in patients imaged with a Siemens Encore2 camera system, suggesting the results are also comparable to conventional SPECT/CT AC results. We also demonstrated closer agreement between AC and DeepAC than AC and NC. While DeepAC is most relevant in centers without hybrid camera systems, it also avoids issues related to misregistration[27] and saves both imaging time and radiation exposure. Image quality for the majority of studies was graded as good, with smaller proportions graded as excellent or fair and less than 2% of cases graded as poor. These gradings are consistent with image quality in routine clinical practice(28), suggesting that our proposed DeepAC approach could be applied to most clinical studies. Therefore, it may also play a role in centers with hybrid SPECT/CT systems.

Our study has a few important limitations. Firstly, we did not have reader scores per segment to allow comparisons of the per-vessel diagnostic accuracy or differences between clinical scores on a segmental basis. However, we did demonstrate higher prediction performance across all vascular territories compared to NC TPD. If our approach was implemented in place of CT-based AC, the reductions in radiation exposure and imaging time would need to be balanced against the potential clinical utility of evaluating coronary artery calcium. Lastly, while our results demonstrated excellent accuracy at a population level, there may still be cases with over or under-correction of attenuation artifacts. Physicians would still

need to review the DeepAC images to identify potential errors, similar to how they perform it for the actual AC images, where guidelines recommend reviewing both NC and AC images(29). For example, abnormal wall motion or the presence of reversible defects could help physicians identify overcorrection in DeepAC image sets. However, this is a potential benefit from a synthetic AC approach that generates SPECT image sets.

## CONCLUSION

In an external population undergoing SPECT MPI on conventional camera systems, the prediction performance for obstructive CAD was higher with DeepAC compared to NC. The improvement in prediction performance was primarily demonstrated in patients undergoing exercise stress. This approach could be applied in sites with conventional SPECT camera systems, which still perform the majority of MPI, to improve diagnostic accuracy and potentially improve patient outcomes.

## CLINICAL PERSPECTIVES

### Competency in Medical Knowledge:

Deep learning-based attenuation correction can improve diagnostic accuracy of conventional single photon emission computed tomography myocardial perfusion imaging.

### Translational Outlook:

Prospective studies are warranted to determine whether this approach can be applied in clinical practice to improve clinical management.

## REFERENCES


1. Gulati M, Levy PD, Mukherjee D et al. 2021 AHA/ACC/ASE/CHEST/SAEM/SCCT/SCMR Guideline for the Evaluation and Diagnosis of Chest Pain. J Am Coll Cardiol 2021 Nov, 78 (22) e187–e285
2. Huang J-Y, Yen R-F, Lee W-C et al. Improved diagnostic accuracy of thallium-201 myocardial perfusion single-photon emission computed tomography with CT attenuation correction. J Nucl Cardiol 2019;26:1584-1595.
3. Ibrahim J, Soman P. The past, present, and future of attenuation correction for myocardial perfusion imaging. J Nucl Cardiol 2023;30:1794-1796.
4. Al-Mallah MH, Bateman TM, Branch KR et al. 2022 ASNC/AAPM/SCCT/SNMMI guideline for the use of CT in hybrid nuclear/CT cardiac imaging. J Nucl Cardiol 2022;29:3491-3535.
5. Gong K, Yang J, Larson PEZ et al. MR-based Attenuation Correction for Brain PET Using 3D Cycle-Consistent Adversarial Network. IEEE Trans Radiat Plasma Med Sci 2021;5:185-192.
6. Chen X, Zhou B, Xie H et al. Direct and indirect strategies of deep-learning-based attenuation correction for general purpose and dedicated cardiac SPECT. Eur J Nucl Med Mol Imaging 2022;49:3046-3060.
7. Hagio T, Moody JB, Poitrasson-Rivière A et al. Multi-center, multi-vendor validation of deep learning-based attenuation correction in SPECT MPI: data from the international flurpiridaz-301 trial. Eur J Nucl Med Mol Imaging 2023;50:1028-1033.
8. Shanbhag AD, Miller RJH, Pieszko K et al. Deep Learning-Based Attenuation Correction Improves Diagnostic Accuracy of Cardiac SPECT. J Nucl Med 2023;64:472-478.
9. Hirschfeld CB, Mercuri M, Pascual TNB et al. Worldwide Variation in the Use of Nuclear Cardiology Camera Technology, Reconstruction Software, and Imaging Protocols. JACC Cardiovasc Imaging 2021;14:1819-1828.
10. Slomka PJ, Betancur J, Liang JX et al. Rationale and design of the REgistry of Fast Myocardial Perfusion Imaging with NExt generation SPECT. J Nucl Cardiol 2020;27:1010-1021.
11. Miller RJH, Lemley M, Shanbhag A et al. The Updated Registry of Fast Myocardial Perfusion Imaging with Next-Generation SPECT. J Nucl Med 2024:jnumed.124.268292.
12. Maddahi J, Agostini D, Bateman TM et al. Flurpiridaz F-18 PET Myocardial Perfusion Imaging in Patients With Suspected Coronary Artery Disease. J Am Coll Cardiol 2023;82:1598-1610.
13. Dorbala S, Di Carli MF, Delbeke D et al. SNMMI/ASNC/SCCT guideline for cardiac SPECT/CT and PET/CT 1.0. J Nucl Med 2013;54:1485-507.
14. Maddahi J, Lazewatsky J, Udelson JE et al. Phase-III Clinical Trial of Fluorine-18 Flurpiridaz Positron Emission Tomography for Evaluation of Coronary Artery Disease. J Am Coll Cardiol 2020;76:391-401.
15. Patel KK, Badarin FA, Chan PS et al. Randomized Comparison of Clinical Effectiveness of Pharmacologic SPECT and PET MPI in Symptomatic CAD Patients. JACC Cardiovasc Imaging 2019;12:1821-1831.
16. Cerqueira MD, Weissman NJ, Dilsizian V et al. Standardized myocardial segmentation and nomenclature for tomographic imaging of the heart. Circulation 2002;105:539-42.
17. Slomka PJ, Nishina H, Berman DS et al. Automated quantification of myocardial perfusion SPECT using simplified normal limits. J Nucl Cardiol 2005;12:66-77.
18. Slomka PJ, Nishina H, Berman DS et al. Automatic quantification of myocardial perfusion stress–rest change: a new measure of ischemia. Journal of Nuclear Medicine 2004;45:183-191.
19. DeLong ER, DeLong DM, Clarke-Pearson DL. Comparing the areas under two or more correlated receiver operating characteristic curves: a nonparametric approach. Biometrics 1988;44:837-45.

20. Chen X, Zhou B, Shi L et al. CT-free attenuation correction for dedicated cardiac SPECT using a 3D dual squeeze-and-excitation residual dense network. J Nucl Cardiol 2022;29:2235-2250.
21. Nguyen TT, Chi TN, Hoang MD, Thai HN, Duc TN. 3D Unet Generative Adversarial Network for Attenuation Correction of SPECT Images. 2020 4th International Conference on Recent Advances in Signal Processing, Telecommunications & Computing (SigTelCom), 2020:93-97.
22. Nye JA. Applying deep learning attenuation correction in the presence of motion. Journal of Nuclear Cardiology 2023;30:1038-1039.
23. Hagio T, Poitrasson-Riviere A, Moody JB et al. "Virtual" attenuation correction: improving stress myocardial perfusion SPECT imaging using deep learning. Eur J Nucl Med Mol Imaging 2022;49:3140-3149.
24. Shanbhag AD, Miller R, Pieszko K et al. Attenuation Correction with Deep Learning-Based Synthetic SPECT Imaging Outperforms Synthetic Polar Maps. J Nucl Med 2023;64:P762-P762.
25. Huang J-Y, Huang C-K, Yen R-F et al. Diagnostic Performance of Attenuation-Corrected Myocardial Perfusion Imaging for Coronary Artery Disease: A Systematic Review and Meta-Analysis. J Nucl Med 2016;57:1893-1898.
26. Burrell S, MacDonald A. Artifacts and Pitfalls in Myocardial Perfusion Imaging. Journal of Nuclear Medicine Technology 2006;34:193-211.
27. Tomita Y, Ishida M, Ichikawa Y et al. The Effect of Misregistration Between CT-Attenuation and PET-Emission Images in 13N-Ammonia Myocardial PET/CT. J Nucl Med Technol 2016;44:73-7.
28. Einstein AJ, Blankstein R, Andrews H et al. Comparison of image quality, myocardial perfusion, and left ventricular function between standard imaging and single-injection ultra-low-dose imaging using a high-efficiency SPECT camera: the MILLISIEVERT study. J Nucl Med 2014;55:1430-7.
29. Dorbala S, Ananthasubramaniam K, Armstrong IS et al. Single Photon Emission Computed Tomography (SPECT) Myocardial Perfusion Imaging Guidelines: Instrumentation, Acquisition, Processing, and Interpretation. J Nucl Cardiol 2018;25:1784-1846.

**FIGURES**

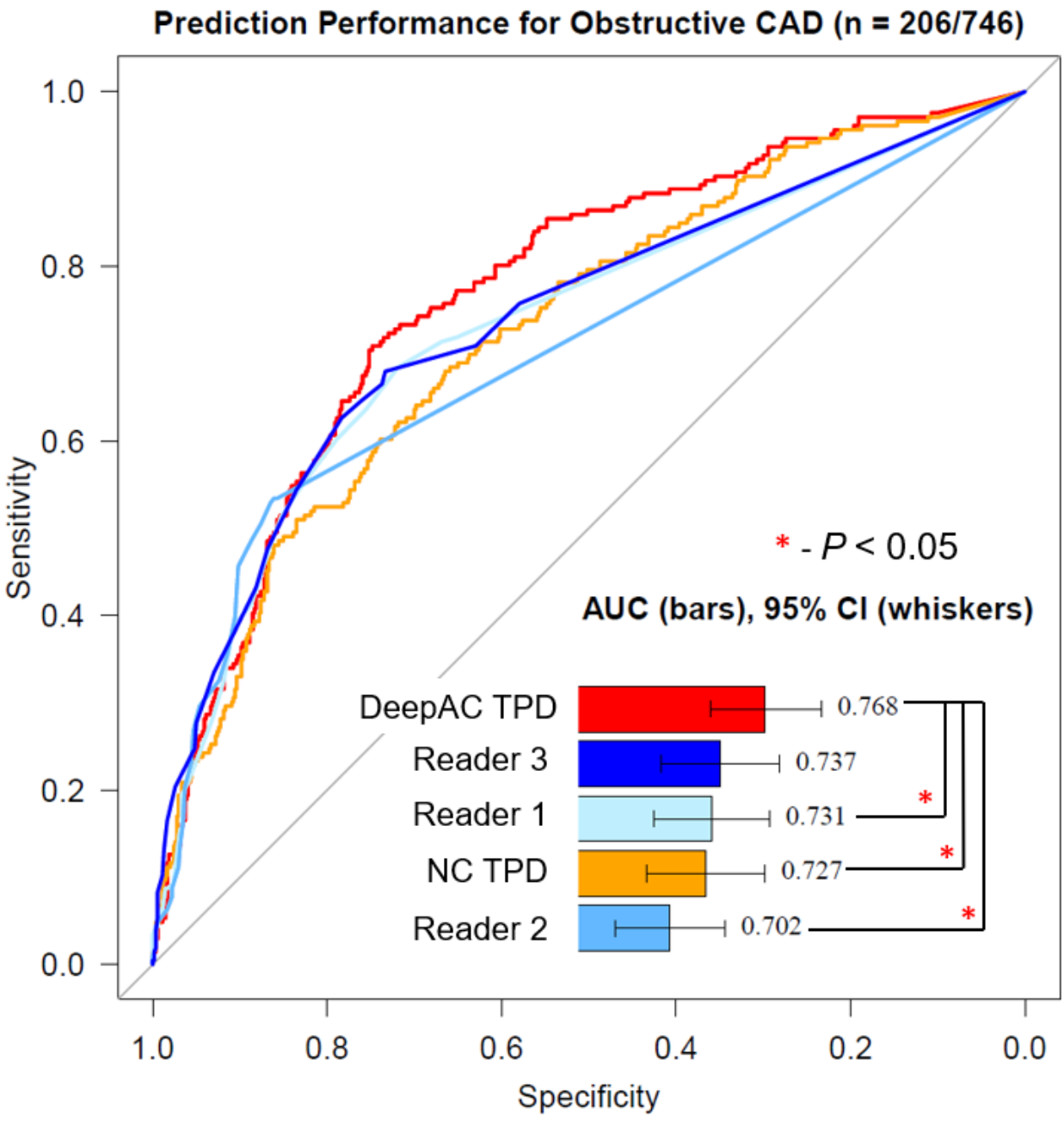


**Figure 1: Overall prediction performance for obstructive coronary artery disease (CAD)**. Attenuation correction (AC) total perfusion deficit (TPD) was derived using deep learning. Obstructive CAD was defined as any stenosis ≥70% or ≥50% in the left main coronary artery in 206 cases out of 746 total patients in the trial. AUC – area under the receiver operating characteristic curve, CI – confidence interval, NC – non attenuation correction.

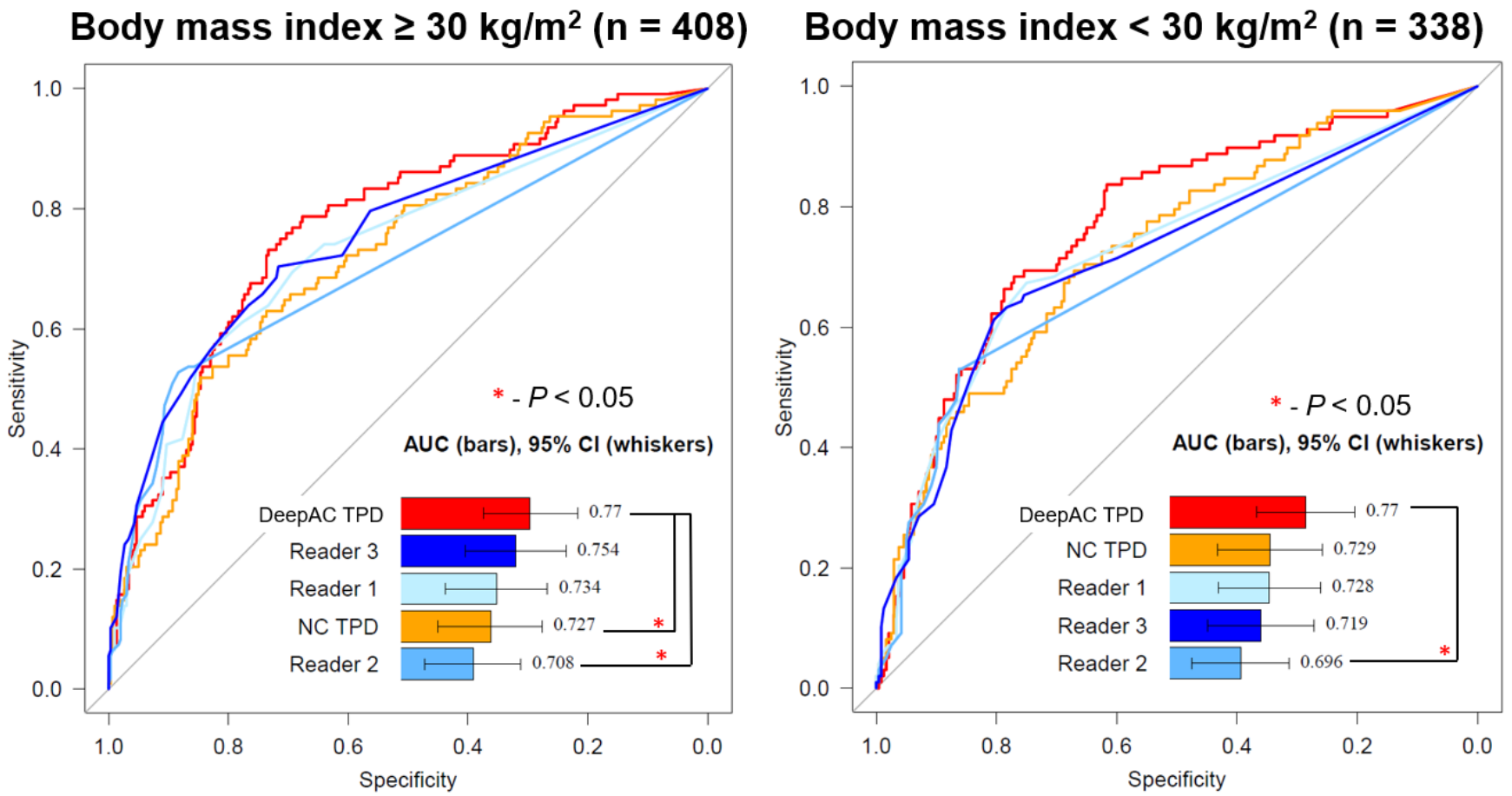


**Figure 2: Obstructive coronary artery disease (CAD) stratified by body mass index (BMI).** Attenuation correction (AC) total perfusion deficit (TPD) was derived using deep learning. Obstructive CAD was defined as any stenosis ≥70% or ≥50% in the left main coronary artery and was present in 108 patients with BMI ≥30 kg/m$^2$ and 98 patients with BMI <30 kg/m$^2$. AUC – area under the receiver operating characteristic curve, CI – confidence interval, NC – non attenuation correction.

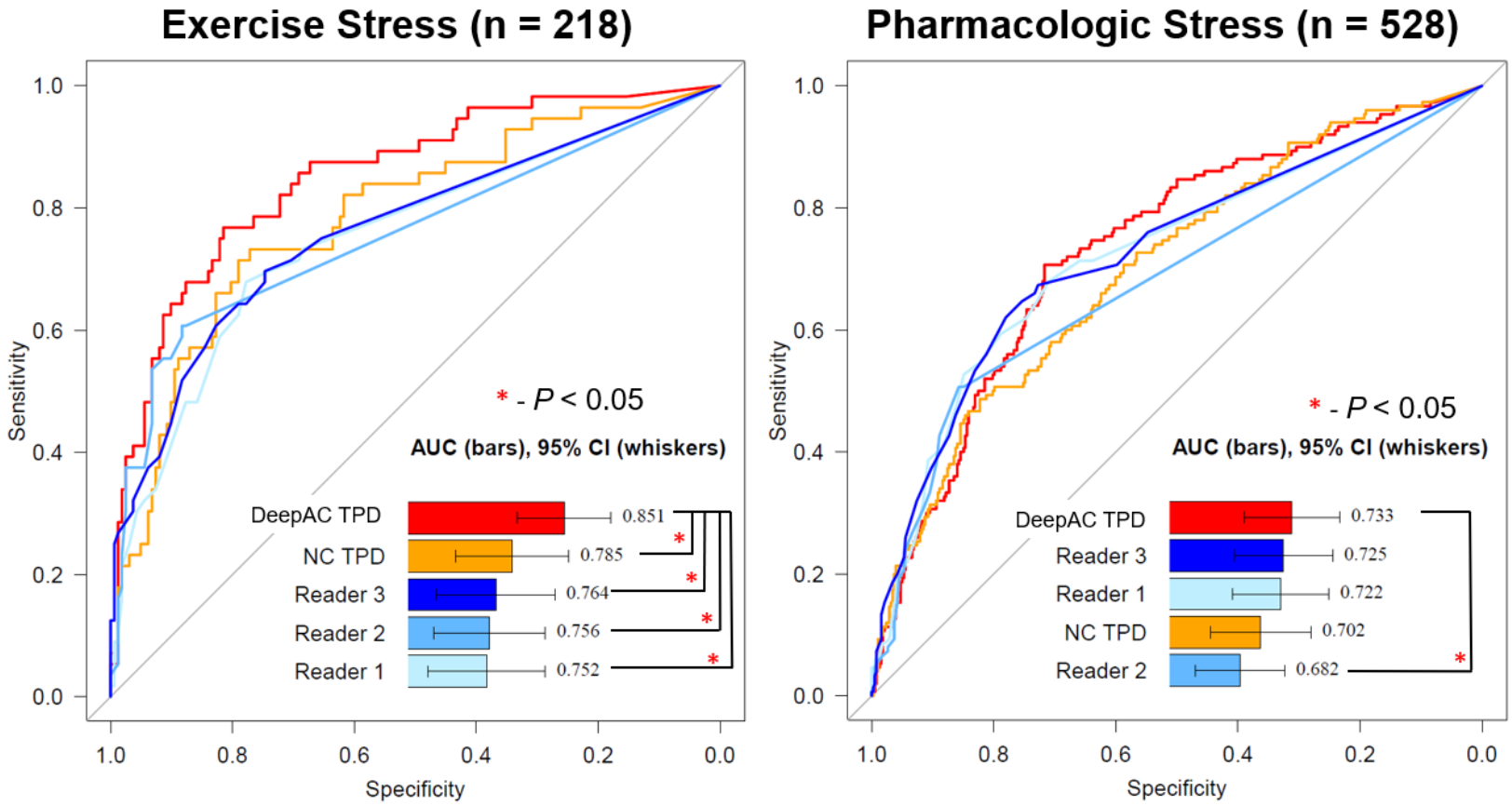


**Figure 3**: **Obstructive coronary artery disease (CAD) stratified by mode of stress.** Attenuation corrected (AC) total perfusion deficit (TPD) was derived using deep learning. Obstructive CAD was defined as any stenosis ≥ 70% or ≥50% in the left main coronary artery. 56 cases with exercise stress had CAD and 150 cases with pharmacologic stress had CAD. AUC – area under the receiver operating characteristic curve, CI – confidence interval, NC – non attenuation correction.

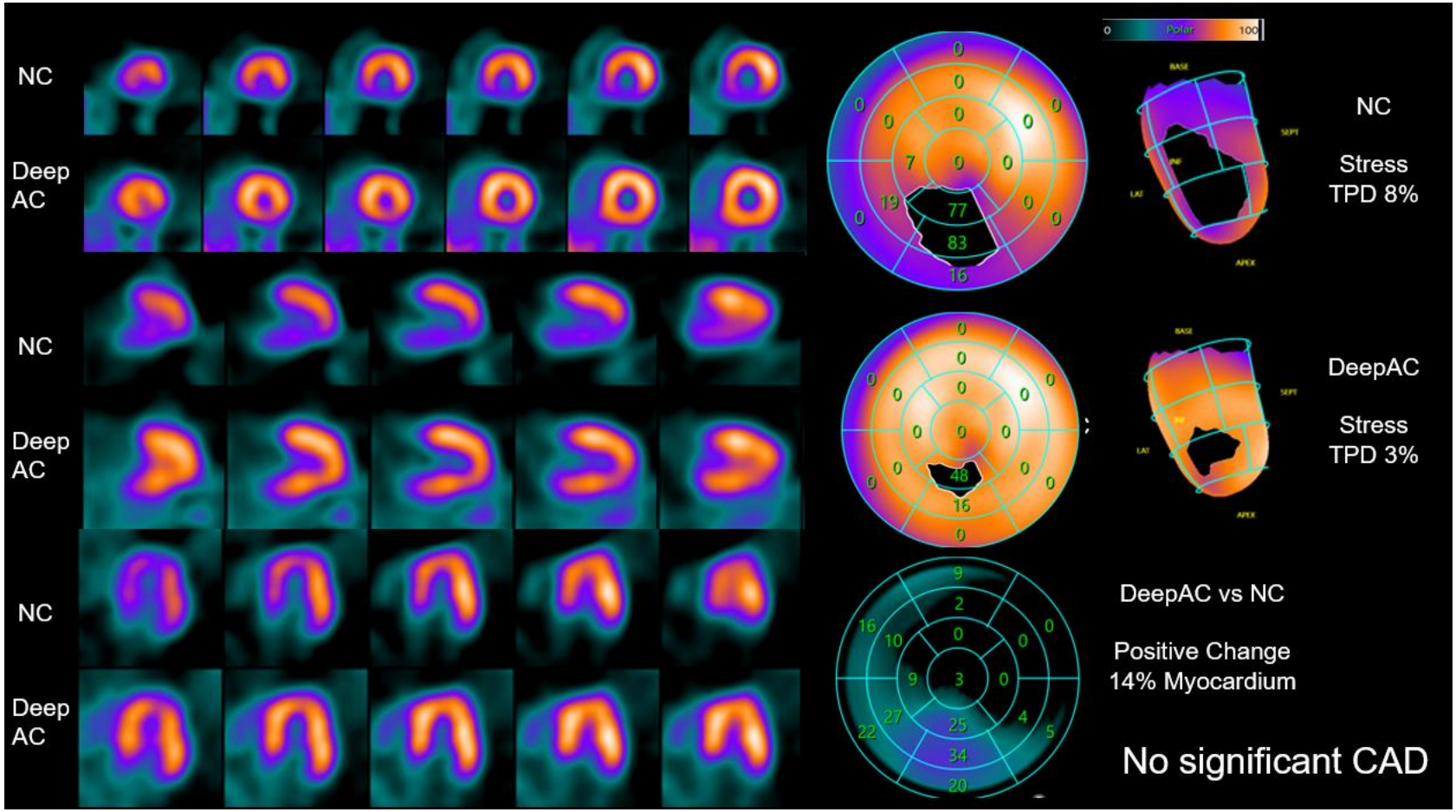


**Figure 4: Case example with no significant coronary artery disease (CAD).** A 61-year-old female patient with body mass index of 30 kg/m$^2$. Non attenuation correction (NC) stress total perfusion deficit (TPD) was abnormal at 8%. One reader interpreted the SPECT NC scan as definitely abnormal and the other two as definitely normal. DeepAC shows only minimal abnormality in the inferior apical segment (3% stress TPD). Invasive coronary angiography demonstrated no obstructive coronary artery disease (maximum stenosis 34% in the left anterior descending artery).

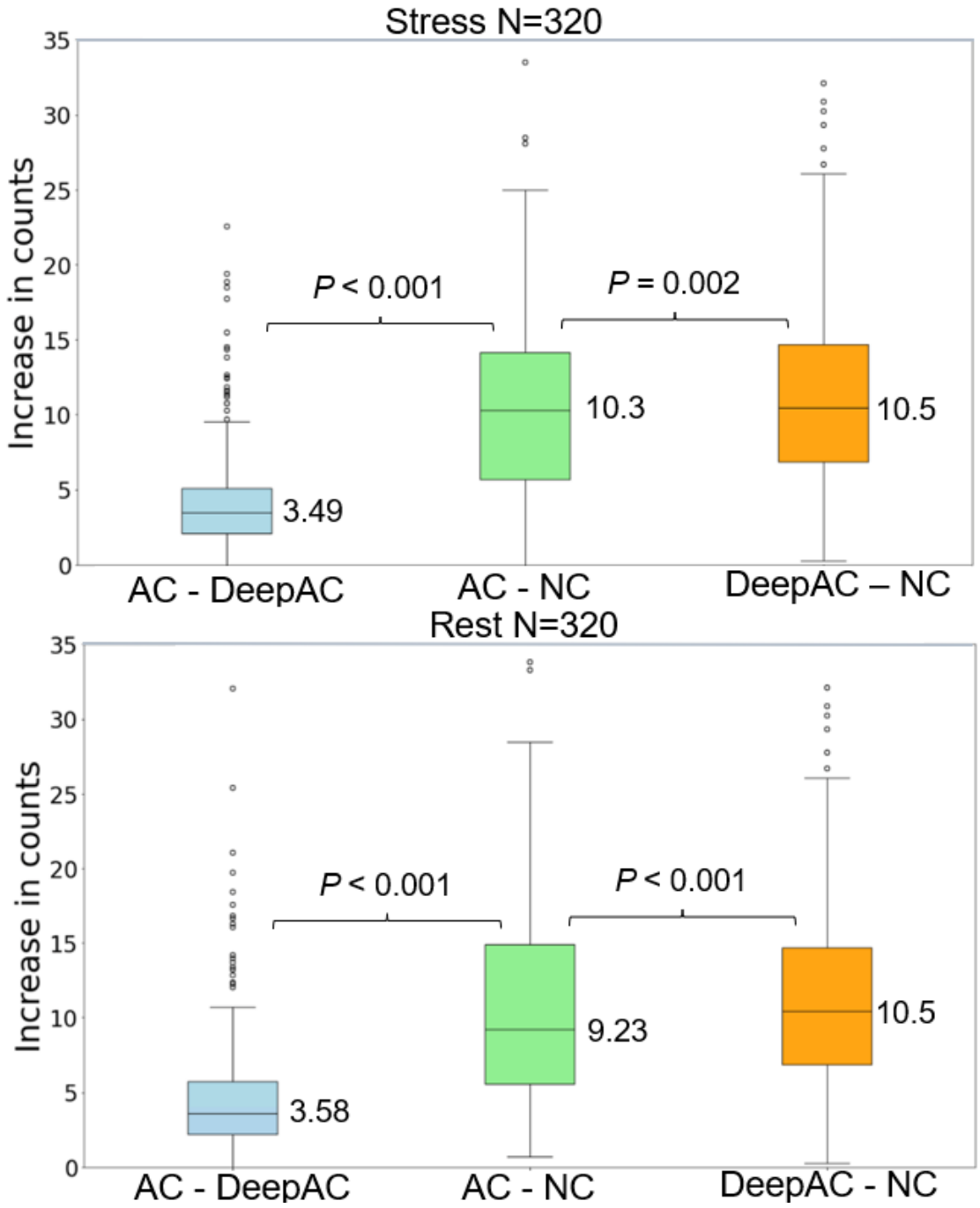


**Figure 5: Change analysis from External Testing Population 2**. Positive change represents an increase in counts on the reference method (listed first) compared to another comparator method (listed second). Positive change was lower for attenuation correction (AC) images compared to DeepAC, relative to the change between AC and non attenuation correction (NC) or DeepAC and NC images on both rest and stress.

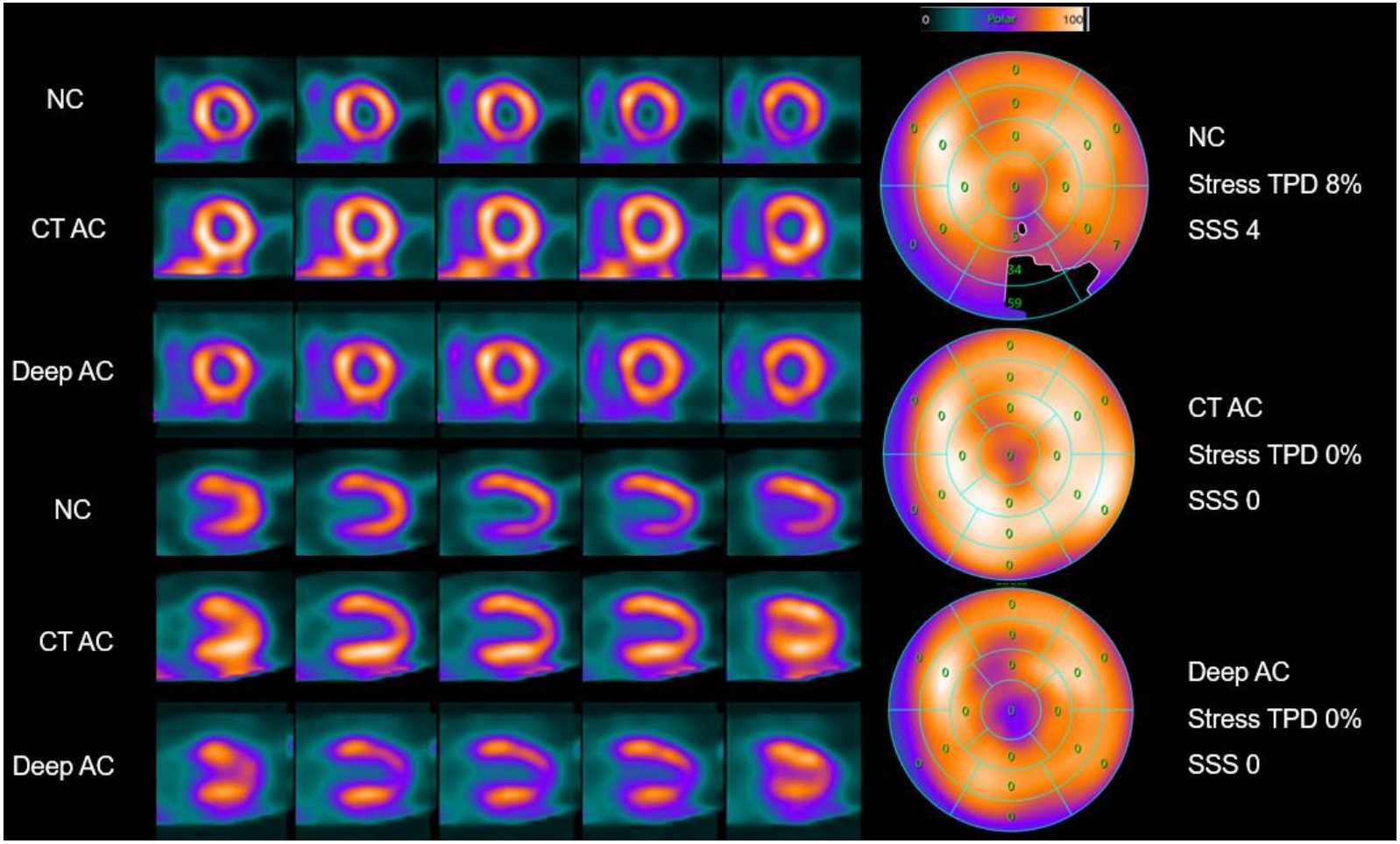


**Figure 6: Case example from External Population 2 with CT Attenuation Correction.** A 57-year-old female patient with high body mass index of 38 kg/m$^2$. Non attenuation correction (NC) total perfusion deficit (TPD) was abnormal at 8% and clinical summed stress score was 4. Both computed tomography (CT) attenuation correction (AC) images and DeepAC images demonstrated minimal perfusion abnormalities (stress TPD 0%, summed stress score [SSS] 0).

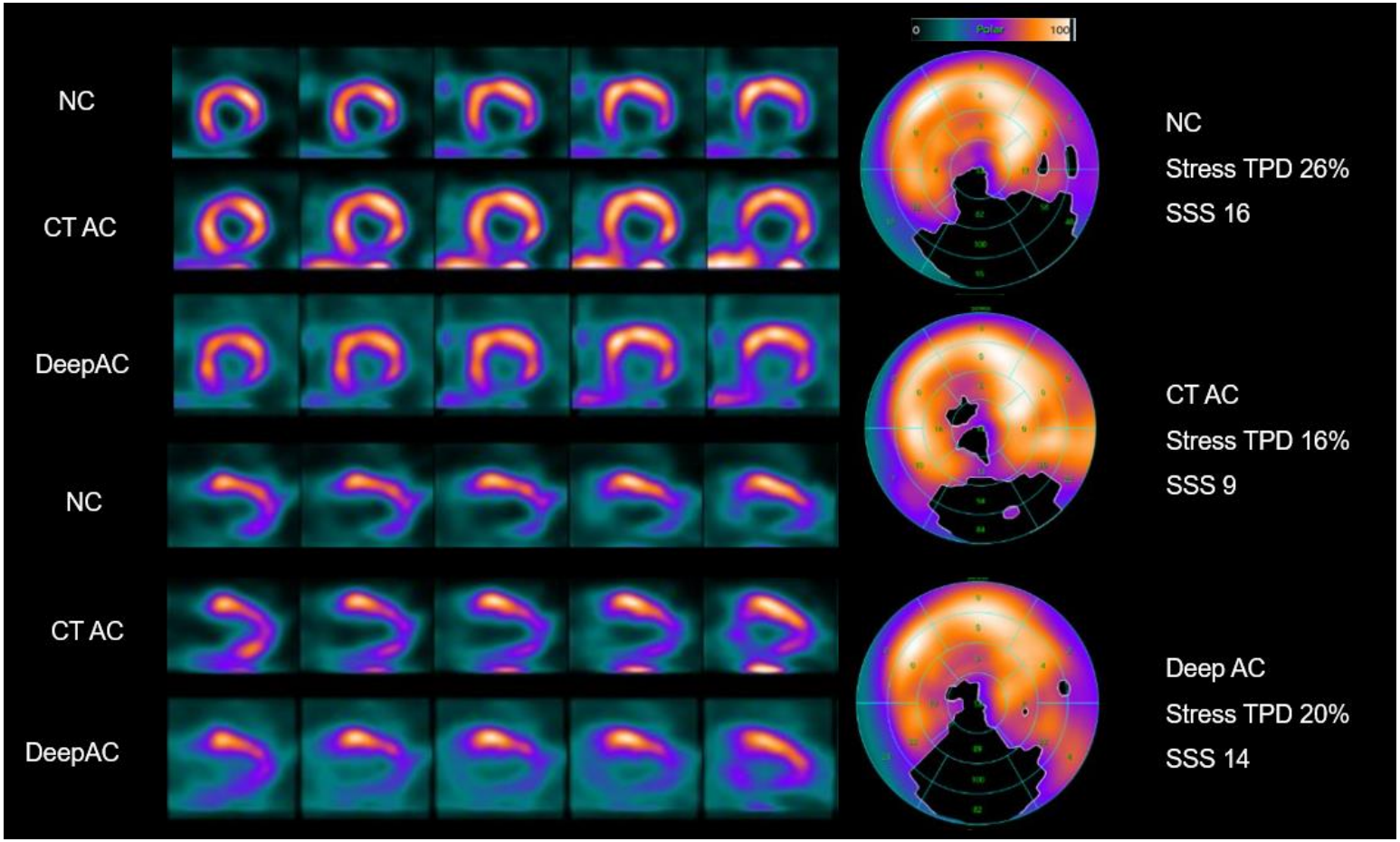


**Figure 7: Defect preservation with DeepAC in case with available CT AC.** A 68-year-old female patient with high body mass index of 52 kg/m$^2$ from External Testing Population 2. All methods for quantitation were abnormal, with summed stress scores (SSS) of 9 for computed tomography-based attenuation correction (CT AC), 14 for DeepAC, and 16 for non attenuation correction (NC) imaging. Reader interpretation was definitely abnormal, with a SSS of 25. Coronary angiography revealed three-vessel disease (100% mid-right coronary artery, 80% mid left anterior descending, and 75% proximal left circumflex).

**Central Illustration: Summary of the Study Methodology**

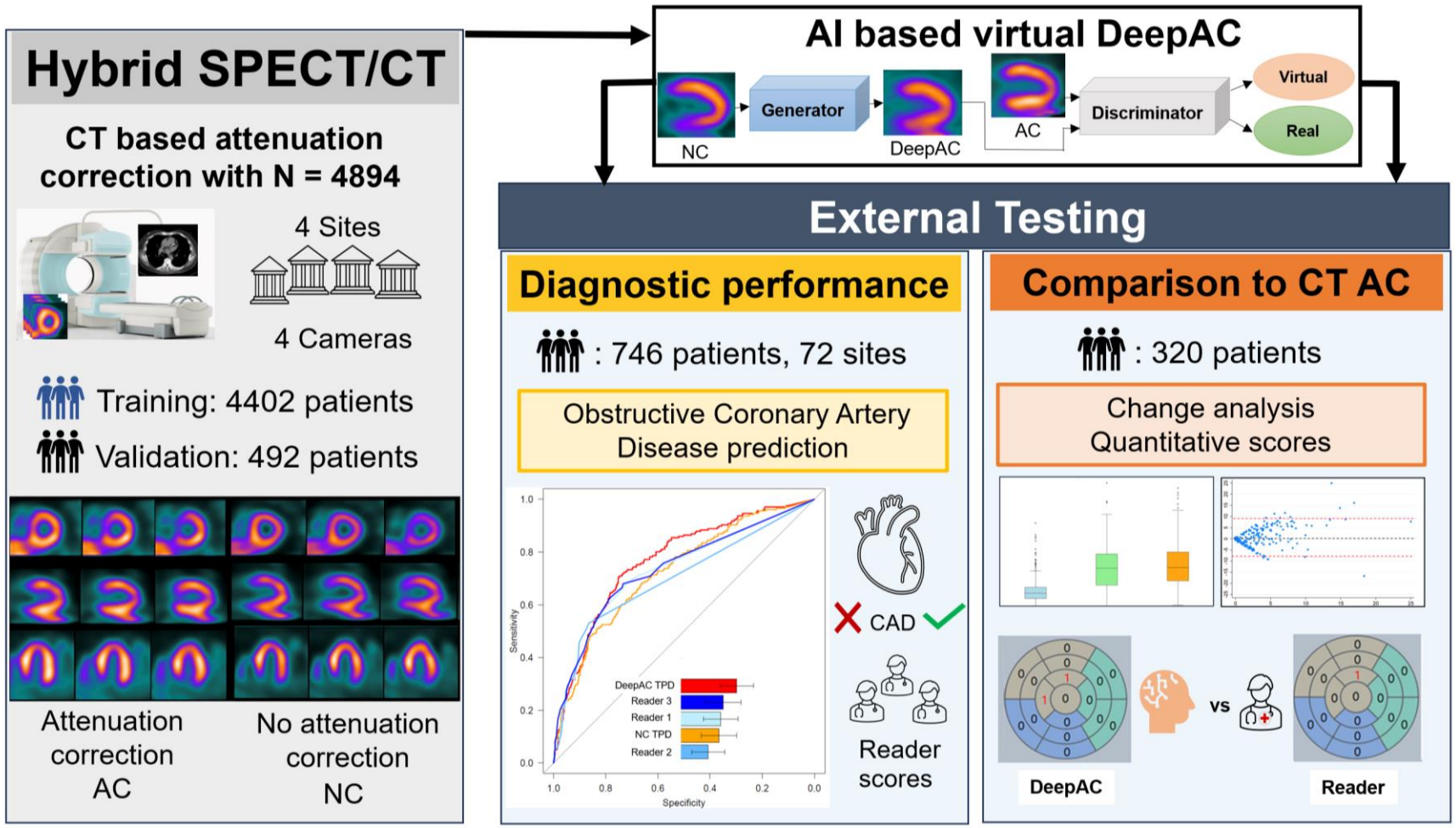


**Central Illustration.** Study Overview. AC – attenuation correction, NC – non attenuation correction, CAD - coronary artery disease, AI - artificial intelligence.

**TABLES**

| | Training and Validation N=4894 | External Testing Population 1 *Phase III Trial* N=746 | External Testing Population 2 *SPECT/CT* N=320 |
|---|---|---|---|
| Age, median (IQR) | 65 (57, 73) | 63 (56, 69) | 61 (54, 68) |
| Male, n (%) | 2523 (52%) | 515 (69%) | 126 (39%) |
| Body mass index, median (IQR) | 31 (27, 35) | 30 (26, 35) | 45 (41, 49) |
| Medical history, n (%) | | | |
| Hypertension | 2568 (52%) | 612 (82%) | 283 (88%) |
| Diabetes | 1046 (21%) | 255 (34%) | 157 (49%) |
| Dyslipidemia | 1716 (35%) | 644 (86%) | 219 (68%) |
| Smoker | 1365 (28%) | 444 (60%) | 27 (8%) |
| Prior myocardial infarction | 447 (9%) | 132 (18%) | 12 (4%) |
| Prior PCI | 423 (9%) | 239 (32%) | 2 (1%) |

**Table 1: Overview of training and validation population as well as external testing populations.** External Testing Population 1 was used to evaluate diagnostic accuracy using data from a phase III multicenter trial. External Testing Population 2 was used to compare DeepAC values to actual AC values. AC – attenuation correction, IQR – interquartile range, PCI – percutaneous coronary intervention.